Journal of Zhejiang University SCIENCE A
ISSN 1673-565X (Print); ISSN 1862-1775 (Online)
www.zju.edu.cn/jzus; www.springerlink.com
E-mail: jzus@zju.edu.cn

Three-dimensional tracking of GLUT4 vesicles in TIRF microscopy*

Xiang-ping WU[†1,2], Jie-yue LI[1], Ying-ke XU[1], Ke-di XU[1], Xiao-xiang ZHENG[†‡1]

([1]*Department of Biomedical Engineering, Zhejiang University, Hangzhou 310027, China*)

([2]*College of Information Engineering, China Jiliang University, Hangzhou 310018, China*)

[†]E-mail: wxp_hzbme@yahoo.com.cn; zxx@mail.bme.zju.edu.cn

Received Dec. 29, 2006; revision accepted Oct. 30, 2007; published online Jan. 10, 2008

Abstract: TIRF microscopy has provided a means to view mobile granules within 100 nm in size in two dimensions. However quantitative analysis of the position and motion of those granules requires an appropriate tracking method. In this paper, we present a new tracking algorithm combined with the unique features of TIRF. Firstly a fluorescence correction procedure was processed to solve the problem of fluorescence bleaching over time. Mobile granules were then segmented from a time-lapse image stack by an adaptive background subtraction method. Kalman filter was introduced to estimate and track the granules that allowed reducing searching range and hence greater reliability in tracking process. After the tracked granules were located in *x*-*y* plane, the *z*-position was indirectly inferred from the changes in their intensities. In the experiments the algorithm was applied in tracking GLUT4 vesicles in living adipose cells. The results indicate that the algorithm has achieved robust estimation and tracking of the vesicles in three dimensions.

Key words: GLUT4, Total internal reflection fluorescence (TIRF) microscopy, Adaptive background subtraction, Kalman filter, Fluorescence correction

doi:10.1631/jzus.A061659 **Document code:** A **CLC number:** TP317.4; Q27

INTRODUCTION

Description of the motion of subcellular granules gives insight in some working mechanisms and structures in living cells. Biologically, microtubules play central roles in the cellular transport and trafficking of many different types of cargos, and meanwhile the long-distance movements of those cargos are shown to be microtubule-dependent (Gross, 2004; Caviston and Holzbaur, 2006).

Two-dimensional (2D) microscopies are usually used to visualize intracellular motion. To explore the depth (*z*-position) information under 2D microscopy, some methods such as confocal imaging technology were based on imaging at different *z*-positions and then analyzed the resulting image *z*-stacks as a function of time (Bornfleth *et al*., 1999; Thomann *et al*., 2002). These methods had a time resolution in the range of seconds and hence could only be applied to slow mobile granules. Additionally, their use in biological applications was limited by high bleaching and photodamage if the imaging time is long. Recently, total internal reflection fluorescence microscopy (TIRFM), exploiting evanescent wave properties to selectively excite image fluorophores in an aqueous or cellular medium very near a glass surface (within 100 nm), has been proved very successful in studying the motion of subcellular granules (Oheim and Stuhmer, 2000; Huet *et al*., 2006). Compared with confocal microscopy, TIRFM has the advantages of lower background disturbance, less bleaching and photodamage and higher temporal resolution (Steyer and Almers, 2001). Under TIRFM, the depth

‡ Corresponding author

* Project supported by the National Natural Science Foundation of China (No. 30770596) and the Key Laboratory for Biomedical Engineering of Ministry of Education of China

offset of a granule to its initial *z*-position can be indirectly inferred from its variation of intensity, since the intensity of the evanescent wave decreases exponentially in the direction orthogonal to the coverslip. In the case of images captured by TIRFM, the intensity is assumed to be constant over time and is only affected by changes in depth and fluorescence bleaching. To exactly calculate the *z*-position, the impact of fluorescence bleaching must be excluded and then a fluorescence correction procedure is consequently demanded to compensate the loss of intensity due to bleaching.

To suppress noise and to achieve tracking stability, tracking is often performed within a Bayesian framework where each object is represented by a state vector evolving along time by biologically realistic dynamic models. The Bayesian tracking allows us to predict the new position of an object knowing its past positions and then seek it in a subsequent frame image within a small region that will save computational consumption and be less sensitive to noise and fake objects. The practical implementation of the Bayesian estimation is usually achieved by some temporal filters such as Kalman filter (Kalman, 1960) and Monte Carlo filter (Isard and Blake, 1998), and these fitters have been widely utilized in biological applications (Genovesio *et al*., 2006; Smal *et al*., 2006; 2007). Temporal filters smooth measured position of object by improving their localization, the measurement being provided by an independent detection algorithm. In the studies of Cheezum *et al*.(2001) and Sbalzarini and Koumoutsakos (2005), different point detection algorithms had been compared and a conclusion was drawn that Gaussian fit was the superior algorithm to locate point objects in terms of both accuracy and precision.

In this study, the long-distance movements of GFP-tagged glucose transporter 4 (GLUT4) vesicles were observed in real-time under TIRFM and a 3D tracking algorithm according to the unique features of TIRFM was put forward. The tracking algorithm consists of fluorescence correction, background subtraction and Kalman filtering, and could be employed to ascertain the role of microtubules in intracellular transportation of GLUT4 vesicles and the mechanisms of GLUT4 transportation in rat primary adipocytes.

FLUORESCENCE CORRECTION

Fluorescence from TIRF microscopy, as excited by argon laser, has time-bleaching character which reflects loss of intensity on fluorescent granules. This time-decaying process is normally assumed to decrease exponentially, which is similar to a depth-decaying process due to scattering and absorption of both excitation and fluorescence light along layers of specimen (Kervrann *et al*., 2004; Schneckenburger *et al*., 2004). So they both can be modeled by an exponential function:

$$\overline{I}_t = \overline{I}_0 \mathrm{e}^{-At}\,|_{t=0,1,\ldots,N_t}, \tag{1}$$

where t denotes the sequence number of a frame image. $\overline{I}_t$ is the average intensity of frame t, $\overline{I}_0$ is the average intensity of the quenchable component before bleaching, and A is exponential rate constant. Then Kervrann *et al*.(2004)'s extended linear model is adopted here on TIRFM sequential images over time:

$$\Delta I_t(L) = I_t(L) - I_{t-1}(L) = -kI_t(L) - m, \tag{2}$$

where $\Delta I_t(L)$ is the numerical approximation of the partial derivative $\mathrm{d}I_t(L)/\mathrm{d}t$ along the time-lapse computed for immediately consecutive two frames, $L=(x, y)$ denotes the spatial coordinates of the 2D discrete images with N pixels, and k and m are the two demanded parameters of this model which are calculated by robust statistical estimation techniques (Kervrann *et al*., 2004). Once k and m are derived, they are used to compute the compensated time-lapse image frames. A restored image $I'_{t+1}(L)$ computed from an original image frame $I_{t+1}(L)$, with reference to an initial frame $I_t(L)$ chosen manually, is obtained. Generally speaking, given an input frame $I_{t+n}(L)$ at time $t+n$ and n successive pairs of estimated parameters $(k_j,\ m_j)|_{j=t,t+1,\ldots,t+n}$, the restored image is warped backwards with reference to the frame t.

The correction approach is the first step of the whole tracking procedure. All the image stacks used in the following were corrected based on the above compensation method.

BACKGROUND SUBTRACTION

Tracking of moving vesicles requires to distinguish the fluorescently tagged moving vesicles. In image sequence analysis, the detection of moving objects is usually easier if a background subtraction procedure is applied (Hayman and Eklundh, 2003; Piccardi, 2004). Background subtraction involves calculating a reference image and subtracting each frame from this image. The simplest form of the reference image is a time-averaged image. This approach suffers from gradual illumination changes in the scene. In the case of images showing fluorescently tagged particles, the global image intensity can vary slowly along time even after fluorescence bleaching compensation. Therefore a simple stationary model for the background is too restrictive and the background subtraction approach used here should be adaptive along time.

(1) Background modeling. It is important to construct a statistical representation of the scene background that supports sensitive detection of mobile granules in the scene. One useful tool for building such representations is statistical modeling, where the intensity values of each pixel over time are modeled as a random variable with an associated probability density function. The density function can be represented parametrically using a normal distribution which is assumed to approximate the actual distribution, with the associated parameters estimated. The mean parameter μ_i and variance parameter σ_i are estimated for each pixel from n sampling frames. In order to obtain a background image without foreground objects, a median is applied for estimation of mean and least trimmed squares (LTS) regression (Ahdesmäki *et al*., 2007) for variance. The central idea behind LTS is that instead of considering complete data set we choose a subset of the signal and use the ordinary least squares regression for the subset.

$$\sigma_i^2 = \frac{2}{n}\min\sum_{s=1}^{n/2}[I_i(s)-\mu_i]^2, \tag{3}$$

where s denotes the subset which corresponds to the $n/2$ lowest values of the measured time points. $I_i(s)$ is the intensity value of pixel i in the sampling frame t.

(2) Foreground extraction. The background model can be used to perform background subtraction as follows. The pixel i at time step t is compared to the model. If $|I_i(t)-\mu_i|>3\sigma_i$, then the pixel is set to foreground. Otherwise it is set to background.

(3) Model update. The background model is adapted on-line using simple recursive updates to cope with scene changes. Adaptation is performed only at image locations that have been labelled as the background region. Recursive estimation of the mean and variance can be performed using the following update equations given the latest measurement $Obs_{i,t+1}$ at time step t+1:

$$\mu_{i,t+1} = \alpha\mu_{i,t} + (1-\alpha)Obs_{i,t+1}, \tag{4}$$

$$\sigma_{i,t+1}^2 = \alpha[\sigma_{i,t}^2 + (\mu_{i,t+1}-\mu_{i,t})^2] + (1-\alpha)(Obs_{i,t+1}-\mu_{i,t+1})^2. \tag{5}$$

These updates estimate a nonstationary Gaussian distribution. The mean and the variance can be time varying. The constant α is set empirically to control the rate of adaptation ($0<\alpha<1$).

KALMAN FILTERING

Tracking can be formalized as a state estimation problem. The tracked object is quantized to a state vector $\boldsymbol{s}\in\mathbb{R}^n$. The goal of tracking is to compute, at each time step, a density function $p(\boldsymbol{s}_t)$ on the state space. In this paper, the state $\boldsymbol{s}_t=(l_x, v_x, l_y, v_y, l_z, v_z)$ includes the position and motion of the object; l_x, l_y and l_z are coordinates of the location; and v_x, v_y and v_z are the instant velocities in the x, y and z directions.

A temporal filter, Kalman filter, is used here to predict and estimate the state of a discrete-time controlled process. The use of a Kalman filter requires a mathematical (state-space) model for the dynamics of the process to be estimated, the target motion in this case. For the time interval between adjacent frames was very small in our experiment, we assumed that the velocity of object is constant between two adjacent frames and may be variable between three or more frames. Accordingly, a simple nearly constant velocity model suffices for the target dynamics. The state-space model is given by:

$$\boldsymbol{s}_t = \boldsymbol{A}\boldsymbol{s}_{t-1} + \boldsymbol{w}_{t-1}, \tag{6}$$

where $\boldsymbol{A} = \mathrm{diag}(\boldsymbol{A}_1, \boldsymbol{A}_1, \boldsymbol{A}_1)$, $\boldsymbol{A}_1 = \begin{bmatrix} 1 & \Delta t \\ 0 & 1 \end{bmatrix}$.

The 6×6 matrix $\boldsymbol{A}$ in the dynamic Eq.(6) is the transition matrix which relates the state at previous time step $t-1$ to the state at the current step t. Δt is the time interval between two adjacent frames.

The use of a Kalman filter requires not only a dynamic model as described above, but also a measurement model for available measurement $\boldsymbol{Ob}\in\mathbb{R}^n$:

$$\boldsymbol{Ob}_t = \boldsymbol{H}\boldsymbol{s}_t + \boldsymbol{u}_t, \tag{7}$$

where $\boldsymbol{H} = \begin{bmatrix} 1 & 0 & 0 & 0 & 0 & 0 \\ 0 & 1 & 0 & 0 & 0 & 0 \\ 0 & 0 & 1 & 0 & 0 & 0 \end{bmatrix}$.

The 3×6 matrix $\boldsymbol{H}$ in the measurement Eq.(7) relates the state to the measurement $\boldsymbol{Ob}_t$. The process noise $\boldsymbol{w}_{t-1}$ with the covariance $\boldsymbol{Q}_{t-1}$ represents the error or innovation in $\boldsymbol{s}_t$ compared to $\boldsymbol{s}_{t-1}$. As the target dynamics model is represented by a nearly constant velocity model, the noise "acceleration" is tiny with a small effect on $\boldsymbol{s}_t$ that accounts for unpredictable modeling errors. Then the covariance $\boldsymbol{Q}_{t-1}$ is assumed to be a very small but non-zero constant vector and similarly for $\boldsymbol{R}_t$, the covariance of the measurement noise $\boldsymbol{u}_t$. The non-zero variances give more flexibility in tuning the filter.

The Kalman filter estimates a process by using a form of feedback control: the filter estimates the process state at some time and then obtains feedback in the form of measurements with noise. As such, the equations for the Kalman filter fall into two groups: time update equations and measurement update equations. The time update equations are responsible for projecting forward (in time) the current state $\boldsymbol{s}_{t-1}$, and error covariance estimates $\boldsymbol{P}_{t-1}$ are used to obtain the a priori estimates for the next time step:

$$\hat{\boldsymbol{s}}_t = \boldsymbol{A}\boldsymbol{s}_{t-1}, \tag{8}$$

$$\hat{\boldsymbol{P}}_t = \boldsymbol{A}\boldsymbol{P}_{t-1}\boldsymbol{A}^{\mathrm{T}} + \boldsymbol{Q}_{t-1}. \tag{9}$$

The measurement update equations are responsible for the feedback, i.e., for incorporating a new measurement $\boldsymbol{Ob}_t$ into the a priori estimate to obtain an improved updated estimate:

$$\boldsymbol{K}_t = \hat{\boldsymbol{P}}_t\boldsymbol{H}^{\mathrm{T}}(\boldsymbol{H}\hat{\boldsymbol{P}}_t\boldsymbol{H}^{\mathrm{T}} + \boldsymbol{R}_t)^{-1}, \tag{10}$$

$$\boldsymbol{s}_t = \hat{\boldsymbol{s}}_t + \boldsymbol{K}_t(\boldsymbol{Ob}_t - \boldsymbol{H}\hat{\boldsymbol{s}}_t), \tag{11}$$

$$\boldsymbol{P}_t = (\boldsymbol{I} - \boldsymbol{K}_t\boldsymbol{H})\hat{\boldsymbol{P}}_t, \tag{12}$$

$\boldsymbol{K}$ is the Kalman gain. After each time and measurement update pair, the process is repeated with the previous a posteriori estimates used to project or predict the new a priori estimates.

To get the measurement value for the Kalman filter, a tracked granule is roughly located firstly in x-y plane. In the x-y image plane, the tracked vesicle is searched in 10×10 ROI. The centre of ROI is predicted by Eq.(8). In this region, the pixel is identified as the centre of tracked granule if its intensity is a local maximum and the number of its neighboring pixels with their intensities around a certain threshold is greater than 4. Here the threshold is determined by the predicted z-position which is also predicted through Eq.(8). The relation between z-position and the intensity of tracked granule will be discussed in the following.

After the tracked granule is roughly located as above, its intensity profile is fitted by a Gaussian profile. An ROI around is selected such that it is both large enough to yield a good Gaussian fit of the target granule, and small enough to prevent the influence of other fluorescent granules on the analysis. The intensity profile is fitted with the following 2D Gaussian function:

$$I(r) = I_0 \exp\left[-\frac{(x-x_0)^2 + (y-y_0)^2}{\sigma^2}\right] + I_{\mathrm{BG}}, \tag{13}$$

x_0, y_0 are regarded as the coordinates of the granule centre and x, y are coordinates of neighboring pixels in the small region. I_{BG} is intensity of the background. Due to prior background subtraction procedure, here the I_{BG} can be set to zero. I_0 and σ are fitted parameters which are yielded by the least-squares approximation.

Granule intensity corresponding to the area under the Gaussian fit is given by $I_{\mathrm{ves}}=I_0\sigma$. Intensity variations along a trajectory, $I_{\mathrm{ves}}(t)$, are obtained by repeating this procedure frame by frame. According to the exponential relationship between the fluorescence intensity of a particle and its vertical position as this granule moves within evanescent field, the vertical position of the particle can be obtained from the changes in granule's fluorescence intensity:

$$z(t) - z_0 = -d\ln\left(I_{\mathrm{ves}}(t)/I_{\mathrm{ves}}(0)\right), \tag{14}$$

where d is the penetration depth of the evanescent wave and z_0, corresponding to the initial position, is an unknown but constant offset for every granule.

EVALUATION ON SIMULATED DATA

To evaluate the tracker, a 3D synthetic image stack consisting of 5 slices separated by 350 nm was built. Tags in the slices generated by the Gibson point spread function (PSF) model (Gibson and Lanni, 1992) were positioned in the image space filled with a dark background (Fig.1), and additive white noise was superimposed to obtain test data at different signal noise ratios (SNR) (Fig.2) which was defined by Eq.(15). The size of every image slice is 256×256 and one pixel denotes 162 nm.

$$SNR = 10 \cdot \lg\left(\sum_{x=1}^{M}\sum_{y=1}^{N} \big(f(x,y)\big)^2 \Big/ \sum_{x=1}^{M}\sum_{y=1}^{N} \big(n(x,y)\big)^2 \right). \quad (15)$$

The tracking algorithm (not including the pre-process steps) proposed in this study was performed in the synthetic image stack and the localization error was calculated as follows:

$$err = \sqrt{\frac{1}{N}\sum_{k=1}^{N} \| \boldsymbol{L}_k - \boldsymbol{L}_k^0 \|^2}, \quad (16)$$

$\boldsymbol{L}_k=(x_k, y_k, z_k)^{\mathrm{T}}$ is the estimated position of the tag, which is the center position of the PSF, and $\boldsymbol{L}_k^0 = (x_k^0, y_k^0, z_k^0)^{\mathrm{T}}$ represents the true tag position known from the simulation settings where the motion in the x-y plane are described by Eq.(6) and the z-positions along the stack are assumed to gradually move away from the coverslip with 350 nm every two slips. Fig.3a displays the total localization error as a function of the SNR and we can see from it that the localization precision can reach the sub-pixel level when the SNR is below 25 (162 nm/pixel). Considering the measurement of z-position is not the same as that in x-y plane, the error in the z-direction is distinguishingly calculated and shown in Fig.3b.

PERFORMANCE ON BIOLOGICAL DATA

As the major insulin-responsive GLUT isoform in adipose cell, GLUT4 vesicles have attracted the focus of researchers in the diabetes field on its regulated translocation (Gross, 2004; Watson *et al*., 2004; Lizunov *et al*., 2005; Caviston and Holzbaur, 2006).

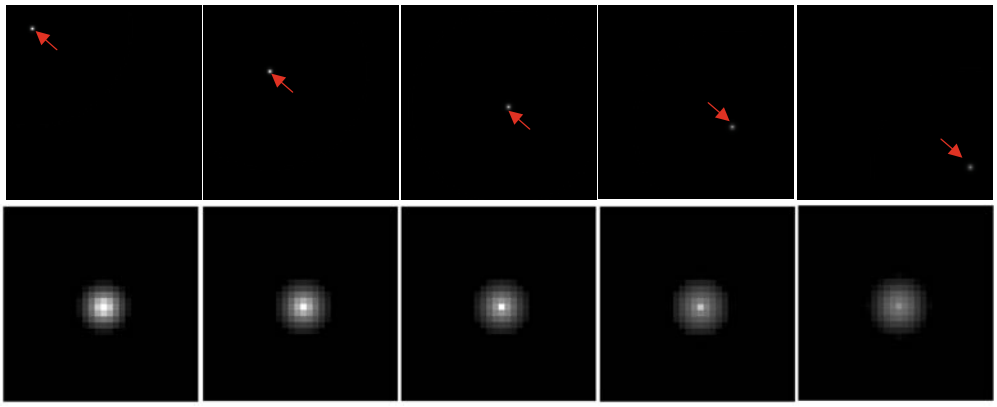

Fig.1 Synthetic image stack. The spots pointed by arrows in the top row denote the moving tags, and their corresponding intensity profiles are shown in the bottom row

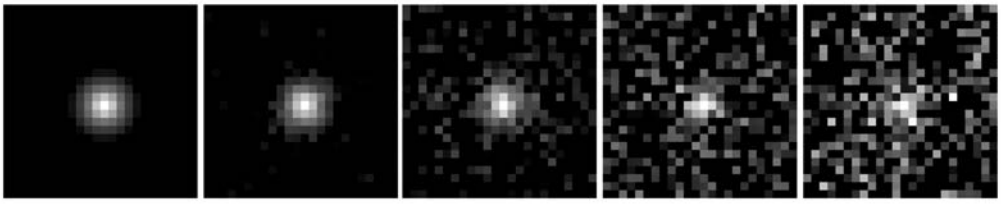

SNR=∞ *SNR*=33 *SNR*=23 *SNR*=16 *SNR*=13

Fig.2 Intensity profile of synthetic spots at different *SNR*

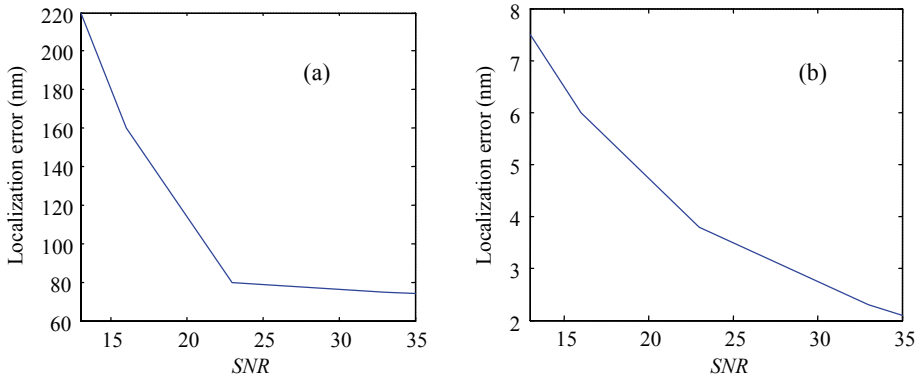

Fig.3 Localization error of the tracking simulation. The horizontal axis denotes the *SNR* and the vertical axis denotes the localization error. (a) Total localization error; (b) Localization error in the *z*-position

In this study, we applied the tracking algorithm in analyzing the long-distance motion of GLUT4 vesicles in adipose cell. Rat primary adipocytes were transfected with the HA-GLUT4-GFP construct and the procedure for monitoring the GFP labelled GLUT4 vesicles was available in (Xu *et al*., 2007).

The Prismless (through-the-objective) TIRF microscopy setup is based on an Olympus IX81 motorized inverted microscope, equipped with an argon laser (excitation λ=488 nm; 10 mW), a 60×1.45 NA oil immersion objective (PlanApoN, Olympus). Penetration depth of the evanescent field was measured to be 100 nm. Time-lapse digital images of ROI were acquired on a cooled CCD camera (iXon, ANDOR Technology), 5 frames per second, under the control of Andor iQ software (Version 1.5, Media Cybernetics, Inc.). The resolution of acquired images is 1004×1002 and one pixel denotes 162 nm. A 257×231 ROI from every frame was cut for post-processing.

Before starting the fluorescence correction procedure, it is necessary to provide a reference frame as a starting point. In our experiment, Frame 1 was chosen manually as the reference frame. As shown in Fig.4, the images in the top row exhibit obvious decrease in intensity due to bleaching, while the restored images (bottom row) keep the intensity changeless.

Fluorescence bleaching over time and *z*-motion are two major factors that affect the intensity of vesicles. The compensation method is robust. On one hand, those spots with drastic lateral displacements or drastic intensity changes between two consecutive frames are excluded as outliers. In this case spatial displacements are the dominant factor contributing to intensity fluctuation, while the effect of fluorescence bleaching is negligible. On the other hand, our correction procedure will compensate those stationary or slowly mobile spots whose intensity changes are more prone to fluorescence bleaching.

Following the fluorescence compensation step, background subtraction was processed to remove the background noise and segment the mobile vesicles. In our experiment, the background model was approximated by the initial 20 frames. The rate of adaptation α, which depends on the frame rate and the rate of change of the viewing field, was manually set to 0.2.

Fig.5c shows that most stationary fluorescent vesicles are filtered. Our adaptive background subtraction method has achieved good results. The method is based on stationary background, so when we observe the specimens under TIRFM, we had better keep the specimens as motionless as possible. Additionally, there will be still some additional salt noise after background subtraction. To further remove them, a median filtering method could be applied.

Based on the background-subtracted image stack, we tracked the vesicle with the Kalman filter. Frame 200 was selected as the starting point of tracking procedure. The object was labelled manually in the starting frame and the remaining steps of the algorithm were fully automatic. We initialized the location components of the state $\boldsymbol{x}_0$ by the center coordinates of the labelled vesicle. All the velocity components were set to zero**.** The process noise covariance $\boldsymbol{Q}$ was assigned a small constant value which was empirical and similarly for $\boldsymbol{R}$ and the initial error covariance $\boldsymbol{P}_0$.

After the *x*-*y* position was located, we could calculate the *z*-position using Eqs.(13) and (14). For z_0 is unknown, we just obtained the relative values to the initial position [Eq.(14)]. Fig.6 gives the illustration of

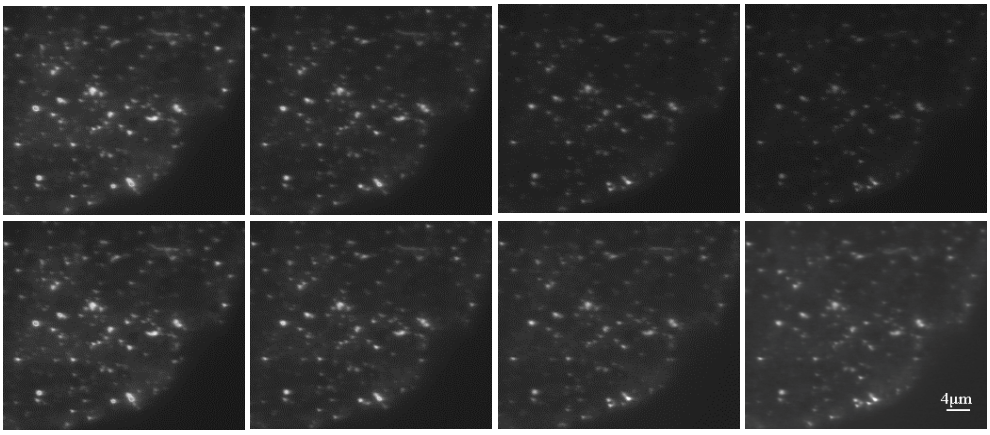

Fig.4 Results of fluorescence correction. Image pairs, from left to right, are Frames 1, 100, 250 and 450. Images in the top row are raw frames and the corresponding restored images by fluorescence compensation are in the bottom row. For comparison, the top row shows the raw images with loss of intensity but no correction for them and the bottom row shows the corresponding results with fluorescence correction procedure

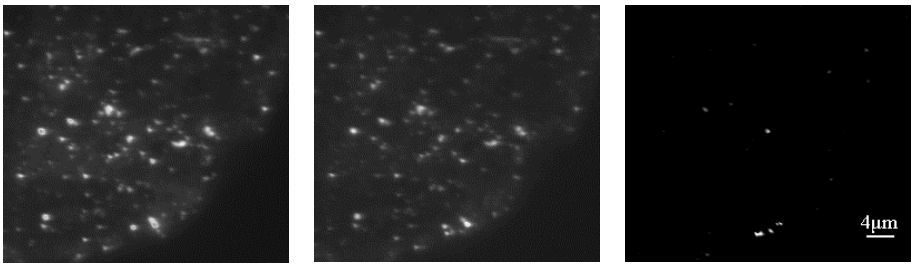

(a) (b) (c)

Fig.5 Results of background subtraction. (a) The image model; (b) The original Frame 220; (c) The subtraction result from (b)

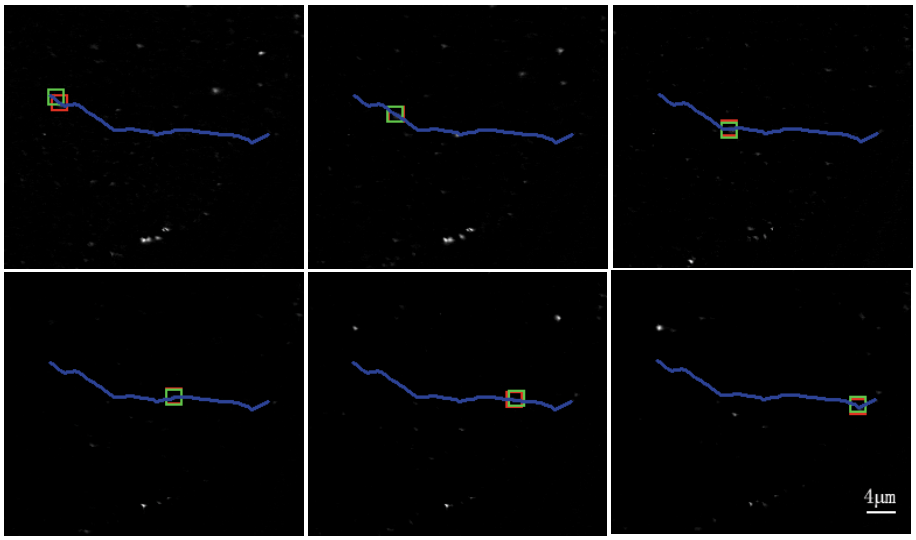

Fig.6 Tracking results of long-distance motion of GLUT4 vesicle. The red rectangle denotes the measured location of the tracked vesicle, the green rectangle denotes the predicted location and the blue line is the moving trajectory of the tracked vesicle. Top row: from left to right are frames 204, 222, 234; Bottom row: from left to right are frames 250, 262, 278

the tracking process in the *x*-*y* image plane. As shown in Fig.6, the mobile vesicle was well tracked and the predicted locations were well coincident with the actually measured locations. Referring to (Lizunov *et al*., 2005), the long-range movement (>10 μm) has the mean speed about 2 μm/s. In our experiment the trace of the mobile vesicle was 32.65 μm and the mean velocity of the vesicle with the radius of 0.57 μm was 2.02 μm/s. The result well corresponds to that reported by Lizunov *et al*.(2005). Also, we applied our method in another experiment with multiple GLUT4 vesicles (Fig.7). In this experiment, the motions of vesicles show various types such as short-distance direct motion (trace 2), random motion (trace 1) and long-distance motion (trace 3).

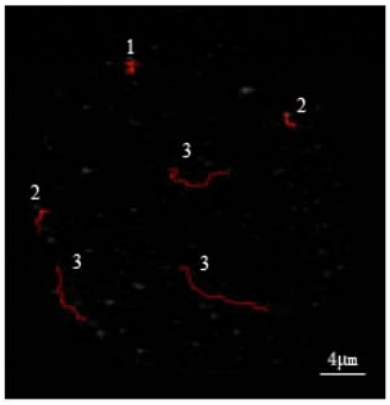

Fig.7 Results of multiple tracking of GLUT4 granules. The red line is the moving trajectory of tracked vesicles and the numbers denote different types of motion
1: random motion; 2: short-distance direct motion; 3: long-distance motion

CONCLUSION

This study aims to present a robust 3D Kalman filter based tracking algorithm to track the GLUT4 vesicles in TIRF microscopy. Through the methods proposed and the experimental results presented above, we concluded:

(1) As there was phenomenon of fluorescence bleaching in our experiments, we have applied a fluorescence correction method to compensate the intensity of vesicle. This procedure was necessary and effective. The following steps, background subtraction and *z*-position measurement, were processed more robustly and accurately owing to the correction method.

(2) According to the acquired images having the complicate background filled with lots of stationary fluorescent vesicles and having gradual changes of intensity, we have adopted an adaptive background subtraction method to remove the stationary vesicles and to segment the mobile ones.

(3) Even after background subtraction, there were some fake mobile vesicles or other true ones belonging to other motion trajectories. Moreover, the tracked vesicles are not speed-invariant. So we have introduced the Kalman filter into tacking process, avoiding searching the whole image space or giving a speed limit. GLUT4 vesicles were well tracked under Kalman filter's prediction-measurement recursive framework.

(4) The fluorescence correction method presented in this study is suitable for other time-lapse fluorescent image stacks and the track algorithm can also be applied in tracking other granules like GLUT4 in living cell.

ACKNOWLEDGEMENTS

We thank Dr. S.W. Cushman with NIH/NIDDK for providing the HA-GLUT4-GFP construct and Dr. Jiangbing Shuai with Zhejiang University for his advice on plasmid purification.

References

Ahdesmäki, M., Lähdesmäki, H., Gracey, A., Shmulevich, L., Yli-Harja, O., 2007. Robust regression for periodicity detection in non-uniformly sampled time-course gene expression data. *BMC Bioinformatics*, **8**(1):233-249. [doi:10.1186/1471-2105-8-233]

Bornfleth, H., Edelmann, P., Zink, D., Cremer, T., Cremer, C., 1999. Quantitative motion analysis of subchromosomal foci in living cells using four-dimensional microscopy. *Biophys. J.*, **77**(5):2871-2886.

Caviston, J.P., Holzbaur, E.L., 2006. Microtuble motors at the intersection of trafficking and transport. *Trends Cell Biol.*, **16**(10):530-537. [doi:10.1016/j.tcb.2006.08.002]

Cheezum, M.K., Walker, W.F., Guilford, W.H., 2001. Quantitative comparison of algorithms for tracking single fluorescent particles. *Biophys. J.*, **81**:2378-2388.

Genovesio, A., Liedl, T., Emiliani, V., Parak, W.J., Coppey-Moisan, M., Olivo-Marin, J.C., 2006. Multiple particle tracking in 3-D+*t* microscopy: method and application to the tracking of endocytosed quantum dots. *IEEE Trans. on Image Processing*, **15**(5):1062-1070. [doi:10.1109/TIP.2006.872323]

Gibson, S.F., Lanni, F., 1992. Experimental test of an analytical model of aberration in an oil-immersion objective lens used in three-dimensional light microscopy. *J. Opt. Soc. Am. A.*, **9**(1):154-166.

Gross, S.P., 2004. Hither and Yon: a rview of bi-directional microtubule-based transport. *Phys. Biol.*, **1**(2):R1-R11. [doi:10.1088/1478-3967/1/2/R01]

Hayman, E., Eklundh, J.Q., 2003. Statistical Background Subtraction for a Mobile Observer. Proc. Ninth IEEE Int. Conf. on Computer Vision (ICCV'03), **1**:67-74. [doi:10.1109/ICCV.2003.1238315]

Huet, S., Karatekin, E., Tran, V.S., Fanget, I., Cribier, S., Henry, J.P., 2006. Analysis of transient behavior in complex trajectories: application to secretory vesicle dynamics. *Biophys. J.*, **91**:3542-3559. [doi:10.1529/biophysj.105.080622]

Isard, M., Blake, A., 1998. Condensation—conditional density propagation for visual tracking. *Int. J. Computer Vision*, **29**(1):5-28. [doi:10.1023/A:1008078328650]

Kalman, R.E., 1960. A new approach to linear filtering and prediction problems. *Trans. ASME—J. Basic Eng.*, **82**:35-45.

Kervrann, C., Legland, D., Pardini, L., 2004. Robust incremental compensation of the light attenuation with depth in 3D fluorescence microscopy. *J. Microscopy*, **214**:297-314. [doi:10.1111/j.0022-2720.2004.01333.x]

Lizunov, V.A., Matsumoto, H., Zimmerberq, J., Cushman, S.W., Frolov, V.A., 2005. Insulin stimulates the halting, tethering, and fusion of mobile GLUT4 vesicles in rat adipose cells. *J. Cell Biol.*, **169**(3):481-489. [doi:10.1083/jcb.200412069]

Oheim, M., Stuhmer, W., 2000. Tracking chromaffin granules on their way through the actin cortex. *Eur. Biophys. J.*, **29**(2):67-68. [doi:10.1007/s002490050253]

Piccardi, M., 2004. Background Subtraction Techniques: A Review. IEEE Int. Conf. on Systems, Man and Cybernetics, **4**:3099-3104. [doi:10.1109/ICSMC.2004.1400815]

Sbalzarini, I., Koumoutsakos, P., 2005. Feature point tracking and trajectory analysis for video imaging in cell biology. *J. Struct. Biol.*, **151**(2):182-195. [doi:10.1016/j.jsb.2005.06.002]

Schneckenburger, H., Gschwend, M.H., Strauss, W.S.L., Sailer, R., Kron, M., Steeb, U., Steiner, R., 2004. Fluorescence lifetime imaging (FLIM) of rhodamine 123 in living cells. *Photochem. Photobiol. Sci*., **3**:127-131. [doi:10.1039/b306129a]

Smal, I., Niessen, W., Meijering, E., 2006. Bayesian Tracking for Fluorescence Microscopic Imaging. Proc. ISBI 2006, p.550-553. [doi:10.1109/ISBI.2006.1624975]

Smal, I., Niessen, W., Meijering, E., 2007. Advanced Particle Filtering for Multiple Object Tracking in Dynamic Fluorescence Microscopy Images. Proc. ISBI 2007, p.1048-1051. [doi:10.1109/ISBI.2007.357035]

Steyer, J., Almers, W., 2001. A real-time view of life within 100 nm of the plasma membrane. *Nat. Rev. Mol. Cell Biol.*, **2**(4):268-276. [doi:10.1038/35067069]

Thomann, D., Rines, D.R., Sorger, P.K., Danuser, G., 2002. Automatic fluorescent tag detection in 3D with super-resolution: application to the analysis of chromosome movement. *J. Microscopy*, **208**(1):49-64. [doi:10.1046/j.1365-2818.2002.01066.x]

Watson, R.T., Kanzaki, M., Pessin, J.E., 2004. Regulated membrane trafficking of the insulin-responsive glucose transporter 4 in adipocytes. *Endocr. Rev.*, **25**(2):177-204. [doi:10.1210/er.2003-0011]

Xu, Y.K., Xu, K.D., Li, J.Y., Feng, L.Q., Lang, D., Zheng, X.X., 2007. Bi-directional transport of GLUT4 vesicles near the plasma membrane of primary rat adipocytes. *Biochem. Biophys. Res. Commun.*, **359**(1):121-128. [doi:10.1016/j.bbrc.2007.05.075]